Controlling Crystallization to Imprint Nanophotonic Structures into Halide Perovskites Using Soft Lithography

Sarah Brittman, Sebastian Z. Oener, Ke Guo, Haralds Āboliņš, A. Femius Koenderink, and Erik C. Garnett*
Center for Nanophotonics, AMOLF, Science Park 104, Amsterdam 1098 XG, the Netherlands

*Corresponding author: garnett@amolf.nl

Abstract

Halide perovskites have recently gained widespread attention for their high efficiencies in photovoltaics, and they have also been studied for applications in light emission. Both of these fields can benefit from nanophotonic patterning. Here, by controlling the crystallization of the perovskite film in contact with a nanotextured silicone polymer stamp, nanostructures are reproduced in the perovskite. Soft lithography techniques such as this imprinting are particularly useful for halide perovskites, which are incompatible with the aqueous solutions and plasmas used in conventional patterning processes. Additionally, soft lithography can pattern over defects and avoids damaging the master. By extending nanoscale soft lithography to halide perovskites, new opportunities arise in merging nanophotonics with these remarkable materials.

Introduction

As a class of materials, halide perovskites have shown exceptional promise for photovoltaics[1] and light emission.[2, 3] In both of these fields, patterning at the nanoscale can improve the performance of devices.[4] In solar cells, patterning increases efficiency through reduced surface reflectance, tailored light trapping, and higher external radiative efficiency and directionality.[5-8] In light emission, nanotexturing raises the outcoupling efficiency and imparts new features such as directionality and spectral tunability.[9] Another common application of nanopatterning is lasing in one- and two-dimensional distributed-feedback (DFB) structures.[10, 11]

Researchers have recently demonstrated a variety of approaches to pattern halide perovskites. The earliest DFB lasers were fabricated by etching the substrate and coating it conformally.[12-16] An alternative approach is to pattern the perovskite directly. Focused ion beam milling has been used to construct textures over small areas,[17] but a scalable technique that takes advantage of the solution-based processing of the perovskite is more desirable. Toward this goal, nanoimprint lithography has been applied to pattern perovskite films through heated and pressurized contact with inflexible stamps.[18-20] This approach has recently been used to produce perovskite DFB lasers.[21] Direct patterning of solution-deposited hybrid perovskites using flexible polydimethylsiloxane (PDMS) stamps was also demonstrated.[22, 23] Unlike a silicon stamp, the PDMS can imprint its textures conformally on non-uniform surfaces and over defects.[24] Also, many PDMS

stamps can be produced from a single master, removing the risk of damaging the expensive master during printing. This method has created large-area arrays of isolated microstructures, but for optoelectronic devices that span the full visible spectrum, such patterning must be pushed to the nanoscale. Toward this goal, 370-nm features have been imprinted into perovskite films using a PDMS stamp and a recrystallization process triggered by exposure to methylamine gas.[23]

Reducing features further, however, requires attention to the integrity of the stamp. Fortunately, the challenges of developing flexible stamps on this length scale have already been addressed by increasing the elastic modulus of the polymer.[24, 25] Features as small as a few nanometers have been replicated in molded polymers such as polyurethane[25-27] and in silica sol-gel films.[24] Imprinting nanoscale features into crystalline materials, such as crystalline polymers, however, is far more challenging because interfaces with the stamp and substrate dramatically influence the crystallization process.[28]

In this work, nanophotonic structures as small as 130 nm are imprinted into perovskite films by crystallizing the film's precursors in contact with a nanotextured polymer stamp. The patterning, as well as the thickness of the underlying film that often serves as a waveguide in actual devices, can be controlled by the design of the initial silicon master and then replicated in the stamp. Recrystallization of the perovskite is found to be critical to the quality of imprinting, and a mixture of solvents (rather than methylamine gas) is used to direct the perovskite's crystallization and control the resulting morphology. These nanophotonic textures can potentially be used to enhance the efficiency of perovskite solar cells, direct the emission of light-emitting diodes, or generate perovskite DFB lasers. Such imprinting techniques are particularly appropriate for halide perovskites because their sensitivity to water and plasma processing makes them incompatible with conventional lithography and etching. In order to develop high quality nanoscale imprinting processes, it is essential to control the crystallization dynamics of the perovskite materials.

Experimental

Solutions of the perovskite precursors

Methylammonium bromide (CH_3NH_3Br) was synthesized and recrystallized using the protocol reported previously.[29] 1 M solutions of precursors in either dimethylformamide (DMF, anhydrous 99.8%, Aldrich) or dimethyl sulfoxide (DMSO, anhydrous ≥99.9%, Aldrich) were prepared in a nitrogen glovebox using CH_3NH_3Br : $Pb(C_2H_3O_2)\cdot 3H_2O$ (≥99.99%, Aldrich) in a 3.05:1 ratio. Powders were weighed outside the glovebox but were dissolved inside. The solutions were stirred and heated to 60°C for 30 minutes to dissolve the precursors and then cooled to room temperature before use. Mixtures were prepared by mixing volume percentages of the cooled 1 M pure solutions.

Fabrication of the tri-layer PDMS stamps

Silicon masters. Silicon masters for the PDMS stamps were fabricated by a combination of e-beam lithography, UV photolithography, and reactive-ion etching. 100 nm of ZEP

520 A (Zeonrex Electronic Chemicals) was spincoated onto hexamethyldisilazane (HDMS)-treated 12 mm x 12 mm silicon substrates. The 100 μm x 100 μm gratings were patterned with a dose between 80-100 μC cm^{-2} (adjusted for the grating dimensions) at 30 keV using electron-beam lithography (Raith e-LINE). After exposure, the resist was developed in pentyl acetate for 30 seconds, followed by rinsing in isopropanol. The gratings were then etched 50-70 nm into the silicon using reactive-ion etching in an Oxford PlasmaPro100 Cobra. The etching recipe started with a brief etch in Cl_2 to remove the native oxide, which was followed by controlled anisotropic etching of the silicon with HBr/O_2. After etching, the substrates were stripped in n-methyl-pyrrolidone to remove the remaining e-beam resist. To produce the waveguide layer underneath the gratings, the gratings were protected in 400 nm of Shipley S1805 photoresist by spincoating at 2000 rpm for 40 seconds and baking at 115°C for 1 minute. UV photolithography was used to expose the surrounding silicon, leaving the gratings underneath strips of resist ~200 μm wide. After the O_2 plasma descum following development of the photoresist, the exposed silicon was etched 140 nm using the same etching process as used for the grating. This has the effect of raising the gratings on top of a 140-nm-thick waveguide (**Fig. S1**). After etching, remaining photoresist was removed in boiling acetone.

Tri-layer stamps. Silicon masters were cleaned with O_2 plasma and then made hydrophobic via vapor-phase silanization using 1H, 1H, 2H, 2H-perfluoro-octyltriethoxysilane (Aldrich). Two compositions of base and curing agent to produce silicone polymers with higher elastic modulus than Sylgard 184 were purchased from Philips International B.V. Base and curing agent for Sylgard 184 (Dow Corning) were used for the backing layer of the stamp.

Approximately 1.5 g of base and curing agent for the intermediate layer (I-PDMS) were mixed in a ratio of 1: 0.18 for 2 minutes and degassed in a vacuum-pumped desiccator for 5 minutes. Then approximately 1.5 g of base and curing agent for the high-modulus layer (X-PDMS) were mixed in a 1: 0.20 ratio for 2 minutes and degassed for 5 minutes.

The silicon masters were first spin-coated with X-PDMS at 2000 rpm (ramp rate 100 rpm/s) for 30 seconds and annealed at 50°C until the layer was only slightly sticky (2-7 mins). Substrates were removed from the heat if the layer is cross-linked too far; otherwise, the adhesion of the subsequent layer fails. Then the substrates were spincoated with I-PDMS at 2000 rpm (ramp rate 200 rpm/s) for 40 seconds and annealed at 50°C for ~30 minutes. Once again, this layer should not be fully cross-linked before adding the final Sylgard 184 layer.

Sylgard 184 was prepared with a 1:10 ratio of the base and curing agent. It was mixed for 8 minutes and degassed for 15 minutes. The substrates coated in X-PDMS and I-PDMS were brought to 70°C on a hotplate. Sylgard 184 was poured onto the heated 12 x 12 mm^2 substrates in the thickest layer possible without breaking surface tension. This thick layer prevents the stamp from curling when it is removed from the silicon master. The Sylgard 184 was annealed for approximately 1 hour to firmness. The substrates were then removed from the hotplate, and the stamps were carefully peeled away. Freeing the edges of the stamps first before peeling helped to prevent tearing of the stamp. Stamps

exhibit a visible curvature because of the tension exerted by the differing elastic moduli and thermal expansion coefficients of the three layers.

Note that masters can be reused to make many stamps. Also, in the case that the PDMS sticks to the masters and cannot be removed by peeling, the master can be recovered by soaking or ultrasonicating it in concentrated H_2SO_4 to remove the silicone polymers.

Imprinting. The stamp was rinsed in DMF, water, isopropyl alcohol, and blown dry with nitrogen gas. It was placed with the textured side up on a hotplate and held at 90°C inside an nitrogen glovebox. 7 x 7 mm^2 fused silica substrates were cleaned in acidic piranha solution (concentrated H_2SO_4: 30% wt. H_2O_2 in a volume ratio of approximately 4:1) at 120°C, rinsed in deionized H_2O and dried with nitrogen gas. They were then further cleaned in an O_2 plasma directly before deposition of the precursor solution. Both steps of this extensive cleaning procedure were necessary for the perovskite solutions to wet the substrates uniformly and reproducibly. The cleaned substrates were transferred inside the glovebox and spincoated with the perovskite precursor solution at 2000 rpm for 60 seconds. The wet film was pre-annealed for the desired amount of time, typically 30-50 seconds for the 4% by volume DMSO mixtures, by holding it face down ~3 mm above the 90°C hotplate. The sample itself was therefore at a much lower temperature than 90°C, and the small gap between the hotplate and sample likely slows the rate of solvent evaporation, allowing fine control of the solvent's removal. During this time, the clear film of precursor changed color to pale orange as the perovskite began to crystallize. Note that the pre-annealing time depended on the composition of the precursor. Longer pre-annealing times were necessary for greater volume fractions of DMSO. For pure DMSO, pre-annealing times of 70-100 seconds were required. After the pre-annealing, the substrate was placed face down into the textured stamp and clamped with a mechanical press exerting a pressure of 200 kPa. Samples were annealed for at least 2 hours under pressure. Then the stamp was peeled away from the surface of the substrate, leaving the imprinted film. Stamps were reused by cleaning; however, after 5-10 uses with precursors in DMF, to which PDMS is slightly permeable, the stamps did need to be replaced for best results.

Characterization

Scanning electron microscopy (SEM) was performed in a FEI Verios 460 using the through-lens detector (TLD). The excitation beam was 5 kV and 100 pA. Some damage to the samples from the electron beam was visible for highly focused images (>80,000X magnification) under these operating conditions.

Atomic force microscopy (AFM) was performed using a Veeco Dimension 3100 in tapping mode using silicon cantilevers (NT-MDT, "Golden" silicon probes NSG01).

Bright- and darkfield optical microscopy were performed using a Zeiss Axio Imager.A2m. For darkfield images displaying the color from diffraction, a 50x objective (Zeis EC Epiplan, NA 0.75) lens was used.

Luminescence measurements from pulsed excitation were performed in a home-built microscope.[30] Briefly, excitation pulses of 0.5 ns at 532 nm (Teem Photonics, STG-03E-1S0) with a maximum energy per pulse ~1 μJ were focused onto the back focal

plane of a NA 0.9 air objective to create wide-field illumination (~60 µm spot diameter) on the sample. The luminescence was collected in reflection, long-pass filtered at 540 nm to remove the excitation beam, and then projected onto the slit of the spectrometer (Shamrock303i spectrometer with Andor Ivac Si CCD detector). For Fourier images of the luminescence, an additional lens was added one focal distance from the back-focal plane of the objective to project the Fourier image onto a thermoelectrically cooled Si CCD camera (Andor CLARA).

The film's absorptance (**Fig. S2**) was measured using a home-built integrating sphere microscopy setup.[29, 31] The sample was mounted inside a 2-inch integrating sphere and illuminated with modulated monochromatic (FWHM 2 nm) light (Fianium WL-SC390-3 with AOTF-V1-N1). The light was focused onto the sample using an objective with low chromatic aberration and long working distance (Mitutoyo M Plan Apo NIR 50X, NA 0.42). The incident, reflected, and transmitted beams were measured via lock-in detection (Stanford Research Systems, SR830) on three different amplified photodetectors (Thorlabs PDA100A).

Photoluminescence (**Fig. S2**) was measured in a WITec alpha300 SR confocal imaging microscope. A 405 nm diode laser (Thorlabs S1FC405) was used to excite the sample, and the luminescence was collected through a NA 0.90 objective. The spectral response of the collection optics, fiber, and spectrometer were calibrated with a standard mercury light source, and the spectrum was corrected accordingly.

Powder X-ray diffraction (**Fig. S2**) was performed in a Bruker D2 Phaser with Cu K-α excitation in a Bragg-Brentano geometry.

Results and Discussion

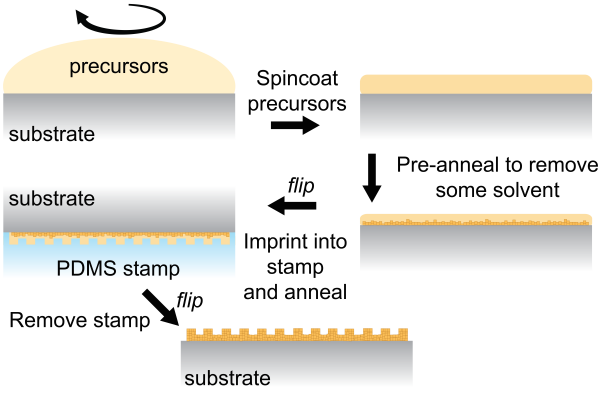

Fig. 1 Scheme depicting the nano-imprinting process.

Because halide perovskites are crystalline materials, patterning them requires controlling their crystallization during processing (**Fig. 1**). To achieve this goal, there are two requirements: (1) uniform coverage across the substrate and (2) controlled recrystallization in contact with the stamp. Since hybrid perovskites are ionic crystals deposited from polar solvents, uniform coverage of the substrate depends sensitively on the preparation of its surface. Commonly, an oxygen plasma is used to produce a hydrophilic, i.e. polar, surface, allowing the polar precursor solution to wet the substrate; however, rapid precipitation is still required to avoid segregation of the film into individual crystals. In previous studies, precipitation has been forced by dripping an anti-solvent such as chlorobenzene or toluene.[13, 32] In this work, it is achieved by a pre-annealing step that increases the supersaturation of the precursor solution and triggers nucleation. One interpretation of this rapid precipitation could be initiation of homogeneous nucleation in the precursor solution, rather than heterogeneous nucleation

on the substrate. After a film has formed, sufficient solvent remains in it to allow further recrystallization in contact with the stamp. If too much recrystallization occurs, however, the perovskite coarsens into isolated crystals as it seeks to reduce its energetically unfavorable interfaces with the substrate (**Fig. S3**). If too much solvent is removed, then the material is not mobile enough to recrystallize in the form of the stamp and little imprinting occurs (**Fig. S4**). As has been demonstrated in substrate conformal imprint lithography (SCIL), these tri-layer stamps reproduce nanoscale features, including those with large aspect ratios; the high elastic modulus of the first layer prevents such features from collapsing.[24]

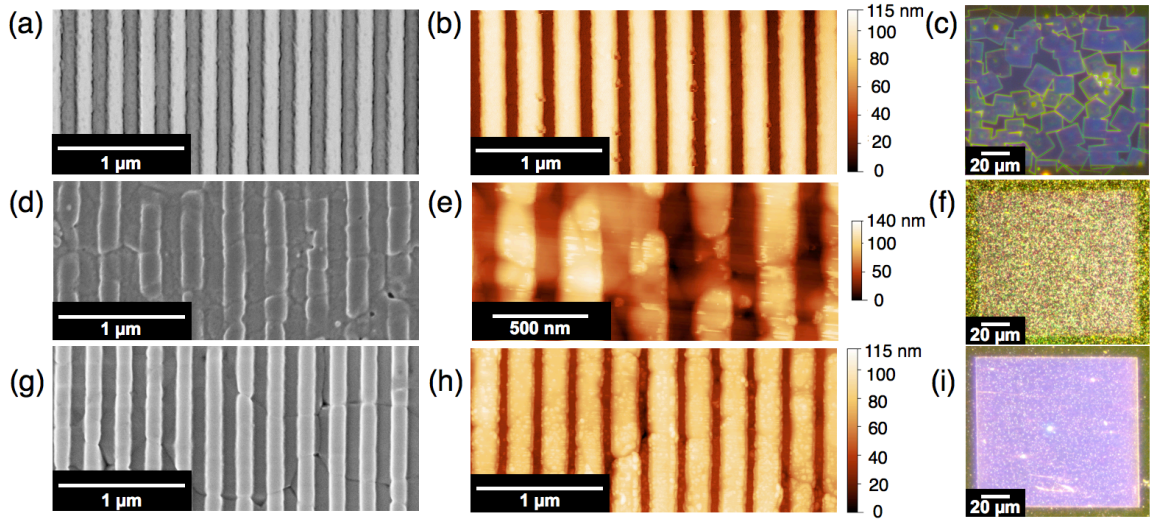

Fig. 2 Effect of solvent on the morphology of the resulting perovskite patterns. SEM (a, d, g), AFM (b, e, h), and darkfield optical images (c, f, i) of $CH_3NH_3PbBr_3$ films prepared from DMSO (a-c), DMF (d-f), and a mixture (4% by volume of DMSO) of the solvents, (g-i). The mixture of solvents provides continuous coverage with high quality features.

Choice of solvent strongly influences the resulting morphology of the patterned perovskite. In general, solutions prepared in dimethyl sulfoxide (DMSO) yield micron-sized crystals or grains whose surface is smoothly imprinted with the stamp, as determined by scanning electron microscope (SEM) and atomic force microscope (AFM) images (**Fig. 2a-c**). Solutions made with dimethylformamide (DMF) produce continuous nanocrystalline films whose patterning follows that of the stamp but with much greater roughness (**Fig. 2d-f**). The difference likely arises because the more rapid drying of DMF during the spincoating and the pre-annealing steps limits the amount of recrystallization that can occur in contact with the stamp. Stamping into wet films of DMF also yields isolated crystals (**Fig. S5**), supporting this hypothesis and showing that this effect is independent of the specific solvent used.

Combining DMF and DMSO along with an optimized pre-annealing step yields continuous films with smoother features, essentially a compromise between the two solvents (**Fig. 2g-i**). A small fraction (4% by volume) of DMSO is added to the precursor solution. During spinning, the solution becomes further enriched in DMSO since DMF evaporates more rapidly. While DMF provides fast crystallization to coat the substrate in a continuous film, the residual DMSO allows the film to recrystallize under the stamp but

not extensively enough to cause the film to aggregate into individual crystals. In films with a non-optimized pre-annealing step, the pattern of recrystallization can be seen centered around wandering lines through the grating (**Fig. 3**). Such lines may indicate paths of escape for the solvent sandwiched between the film and the stamp, which is impermeable to DMSO. If the pre-annealing time is shortened, these lines widen and merge into recrystallization over the entire structure, producing the desired continuous grating (**Fig. S6**).

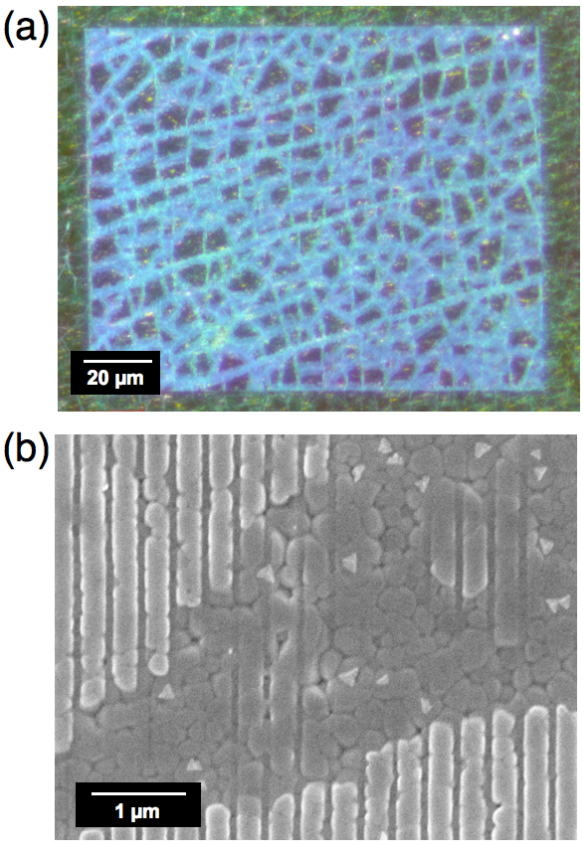

Fig. 3 Partial recrystallization of a perovskite grating. a) Darkfield optical image showing that recrystallization into the grating (blue) occurs along wandering lines within the patterned area. b) SEM image of the regions under the stamp where the grating formed (blue in optical image) and where recrystallization was not sufficient to form the grating (black in optical image).

This approach also works using only DMSO as the solvent, or using mixtures with more than a 4% volume fraction, provided a sufficiently long pre-annealing step is included to limit recrystallization (**Fig. S7**). One drawback, however, is that DMSO-rich solutions of the lead acetate and methylammonium bromide precursors do not wet the substrate as well as mixtures of DMF and DMSO, often yielding discontinuous films. Enhanced cleaning procedures or chemical functionalization of the substrate might overcome this challenge. This method also shows promise for imprinting $CH_3NH_3PbI_3$ (**Fig. S8**), although the solvent mixture and procedure must be optimized for the material's differing crystallization dynamics. Using pure DMSO would also likely reduce swelling and damage to the stamp, since PDMS is impermeable to DMSO.

In evaluating any imprinting method, two key metrics are the size of features produced and their fidelity to the master pattern. For one-dimensional gratings, perovskite wires as thin as 134 nm have so far been achieved, although the resolution limit of the method has not yet been tested systematically. The grating periodicity in the perovskite was systematically larger than that of the silicon master by 4-10% (**Table S1**). Since the tri-layer PDMS stamps are under tension because of the differing elastic moduli between the layers, this stretching of the stamp likely contributes to the expanded features in the perovskite. The height of the imprinted nanoscale features reproduced the depth of the stamp. Other nanoscale structures have also been imprinted into $CH_3NH_3PbBr_3$ films, including inverted pyramids, hole arrays, and individual nanowires (**Fig. 4**).

The hybrid perovskite film formed during patterning exhibits the structure, optical absorption, and photoluminescence characteristic of $CH_3NH_3PbBr_3$ (**Fig. S2**). As expected, the patterned structures strongly modify how light interacts with the film.[30] Darkfield microscope images show the structural color created by first-order diffraction from the grating (**Fig. 2c,f,i**). Colors shift from purple to blue with periodicities ranging from 247 to 333 nm. The uniformity of the color indicates a lower density of structural defects or variations in thickness within the patterned area. Viewing the gratings in the darkfield microscope offers a simple and quick way to assess their quality and to locate them.

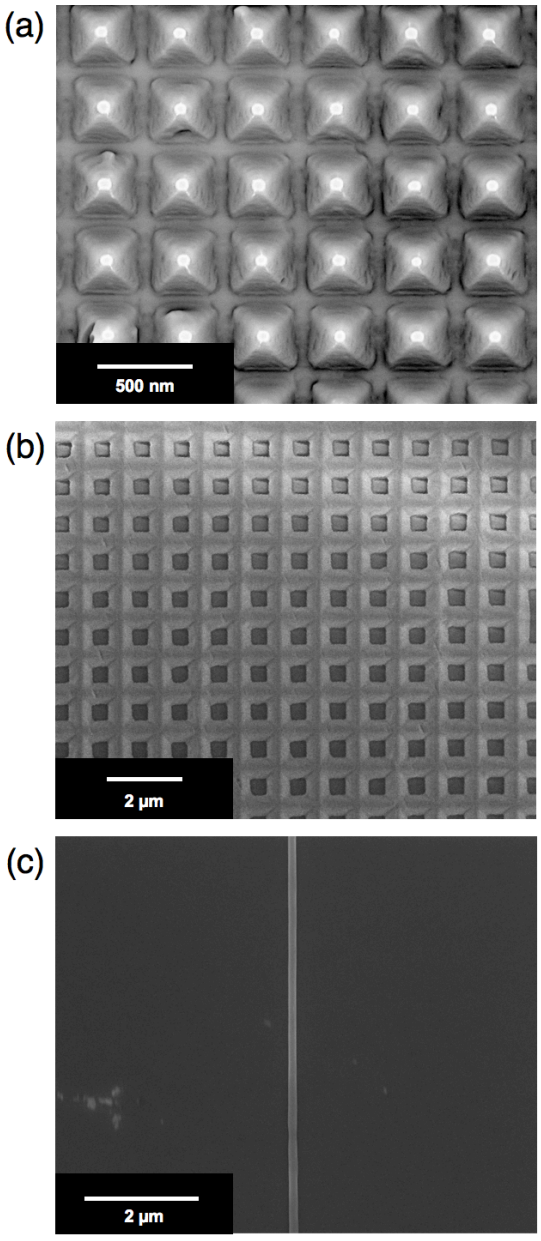

Fig. 4 A variety of nanophotonic structures imprinted into $CH_3NH_3PbBr_3$ deposited from DMSO. a) Inverted pyramids, b) array of square holes, c) single nanowire with a diameter of 130 nm.

The grating also modifies the angular distribution of the photoluminescence from the film (**Fig. 5a**). By collecting the luminescence using an objective with a high numerical aperture (NA=0.90) and imaging its back focal plane, a technique known as Fourier microscopy,[30, 33] it is clear that the grating directs the luminescence into arcs of preferred angles of emission. Adjusting the period of the grating or the thickness of the underlying film that acts as a multimode waveguide tunes the positions of these arcs. The waveguide here supports a transverse electric (TE) and transverse magnetic (TM) mode, each with a different effective index. From the curvature of the arcs, the effective indices (n_{eff}) are determined to be 1.99 and 1.79, which agree well with the estimated mode indices of the 190-nm thick corrugated waveguide: 1.92 and 1.78 (Electronic Supporting Information).

Such a grating structure forms a distributed feedback system that is often used to generate lasing.[34, 35] To satisfy the second-order Bragg diffraction condition, the period of the grating should match the wavelength of the waveguided light (λ_{air}/n_{eff}), where λ_{air} is the wavelength of the light in air. In this case there is feedback between the guided waves traveling in the plane of the film in the direction of the grating and they are diffracted out of the structure normal to the plane. In the Fourier image, the second-order Bragg condition is satisfied when the rings appear to touch in the center of k-space (**Fig. 5a**).

The perovskite gratings show amplified spontaneous emission, but their emission linewidths remain relatively broad. The gratings

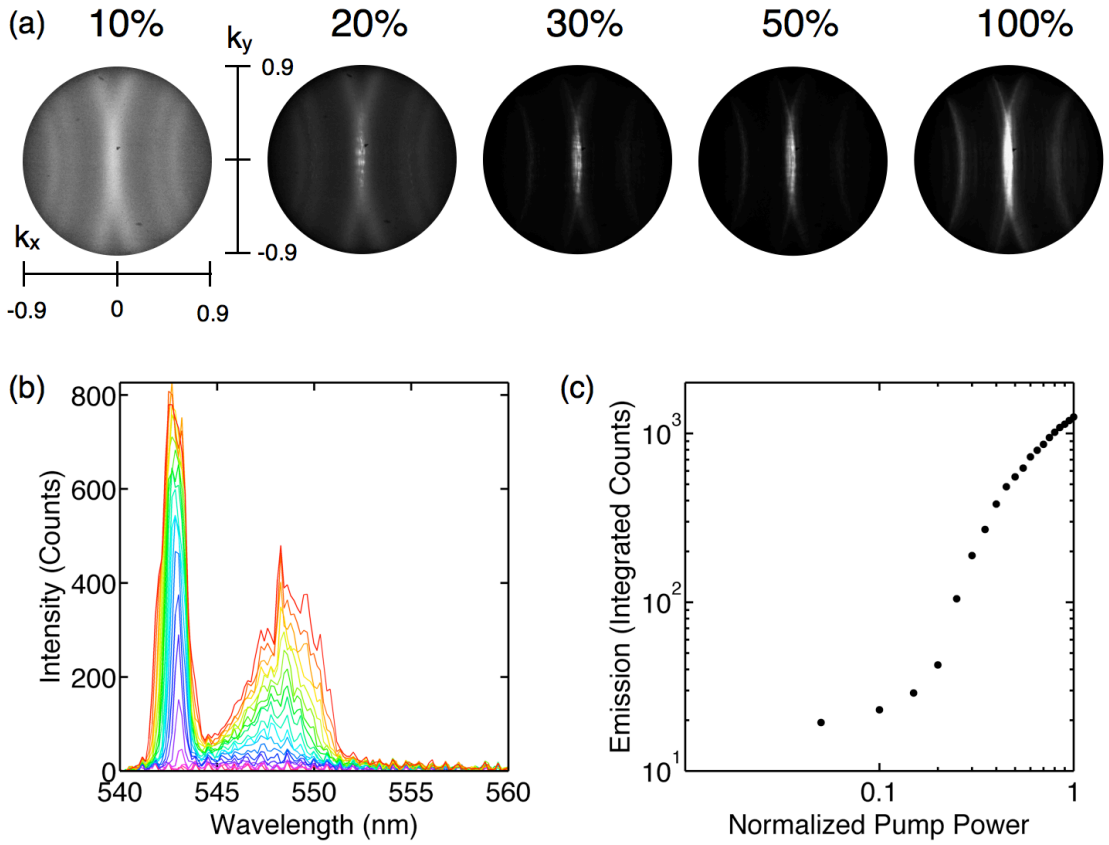

Fig. 5 Photoluminescence (PL) of a $CH_3NH_3PbBr_3$ grating. a) Fourier images of the angular distribution of the emission (plotted on a linear scale) at increasing percentages of the maximum pump power, approximately 1 mJ cm^{-2}. b) Spectra of the PL from low (purple) to high (red) pump powers in steps of 5%. c) The emission of the narrow peak (540-544 nm) integrated as a function of pump power. The kink indicates the transition from spontaneous emission to amplified spontaneous emission.

were excited by single, 0.5 ns pulses from a 532 nm laser over a spot with a diameter of 60 μm. The peak energy of the pulse was approximately 1 μJ. As the pump power increases, the linewidth at first narrows from a full-width half maximum of 17 nm (**Fig. S2**) to 0.5 nm (**Fig. 5b**), and the angular distribution of the light collapses around the center of k-space (**Fig. 5a**); however, these linewidth and angular dispersion are larger than those of other reported perovskite lasers.[13, 14, 21] Also, further increasing the pump power causes the peak to blue shift and broaden, contrary to the behavior of a conventional laser[35] (**Fig. 5b**). Since this behavior is repeatable on each sample, it does not arise from damage to the material or grating structure. Also at these higher powers (>35%), a second peak grows in at longer wavelengths (~548 nm). Gratings with slightly larger pitch matched to this red region also showed narrowed emission, but these too failed to achieve linewidths expected of lasing and also broadened and blueshifted with increasing excitation. Changes in the refractive index at high carrier densities[36] might be responsible for this systematic shift. Imperfections in the grating would make the changes in refractive index nonuniform and could then explain the broadening of the peak at higher excitation power. The characteristic change in slope of the plot of the emitted light

vs. incident pump power appears as the mechanism of emission transitions from spontaneous emission to stimulated emission (**Fig. 5c**). This performance suggests the potential of these gratings to produce lasing, but further optimization is necessary to achieve it in practice. So far imprinted perovskite lasers have used 2D photonic crystals rather than 1D gratings to achieve sufficient feedback to overcome the losses in the structure.[21]

Conclusions

In summary, nanophotonic patterns have been imprinted into halide perovskite films using soft lithography. Controlling the crystallization dynamics of the film can tune the morphology of these structures and be used to extend this method to other solution-processable halide perovskites. Further understanding of these dynamics and the development of chemical means to control them will likely improve the quality and spatial extent of the patterned areas. These nanophotonic structures tailor the optical properties of the perovskite film and can therefore be used to enhance the performance of perovskite optoelectronics such as solar cells, light-emitting diodes, and lasers.

Acknowledgements

The authors thank Dimitry Lamers for advice on fabrication of the silicon masters. The authors acknowledge financial support from the European Research Council under the European Union's Seventh Framework Programme (FP/2007-2013)/ERC Grant Agreement no. 337328, "NanoEnabledPV," and from an industrial partnership between Philips and AMOLF. This work is part of the research program LEDMAP with project number 12754, which is financed in part by the Netherlands Organization for Scientific Research (NWO).

References

1. S. D. Stranks and H. J. Snaith, *Nat. Nanotechnol.*, 2015, **10**, 391-402.
2. B. R. Sutherland and E. H. Sargent, *Nat. Photonics*, 2016, **10**, 295-302.
3. S. A. Veldhuis, P. P. Boix, N. Yantara, M. Li, T. C. Sum, N. Mathews and S. G. Mhaisalkar, *Adv. Mater.*, 2016, **28**, 6804-6834.
4. M. L. Brongersma, Y. Cui and S. Fan, *Nat. Mater.*, 2014, **13**, 451-460.
5. S. Mokkapati and K. R. Catchpole, *J. Appl. Phys.*, 2012, **112**, 101101.
6. Y. Cui, D. van Dam, S. A. Mann, N. J. van Hoof, P. J. van Veldhoven, E. C. Garnett, E. P. Bakkers and J. E. Haverkort, *Nano Lett.*, 2016, **16**, 6467-6471.
7. S. A. Mann, R. R. Grote, R. M. Osgood, Jr., A. Alu and E. C. Garnett, *ACS Nano*, 2016, **10**, 8620-8631.
8. J. M. Richter, M. Abdi-Jalebi, A. Sadhanala, M. Tabachnyk, J. P. Rivett, L. M. Pazos-Outon, K. C. Godel, M. Price, F. Deschler and R. H. Friend, *Nat. Commun.*, 2016, **7**, 13941.
9. A. I. Zhmakin, *Phys. Rep.*, 2011, **498**, 189-241.

10. V. Navarro-Fuster, I. Vragovic, E. M. Calzado, P. G. Boj, J. A. Quintana, J. M. Villalvilla, A. Retolaza, A. Juarros, D. Otaduy, S. Merino and M. A. Díaz-García, *J. Appl. Phys.*, 2012, **112**, 043104.
11. M. Meier, A. Mekis, A. Dodabalapur, A. Timko, R. E. Slusher, J. D. Joannopoulos and O. Nalamasu, *Appl. Phys. Lett.*, 1999, **74**, 7-9.
12. Y. Jia, R. A. Kerner, A. J. Grede, A. N. Brigeman, B. P. Rand and N. C. Giebink, *Nano Lett.*, 2016, **16**, 4624-4629.
13. S. Chen, K. Roh, J. Lee, W. K. Chong, Y. Lu, N. Mathews, T. C. Sum and A. Nurmikko, *ACS Nano*, 2016, **10**, 3959-3967.
14. G. L. Whitworth, J. R. Harwell, D. N. Miller, G. J. Hedley, W. Zhang, H. J. Snaith, G. A. Turnbull and I. D. Samuel, *Opt. Express*, 2016, **24**, 23677-23684.
15. M. Saliba, S. M. Wood, J. B. Patel, P. K. Nayak, J. Huang, J. A. Alexander-Webber, B. Wenger, S. D. Stranks, M. T. Horantner, J. T. Wang, R. J. Nicholas, L. M. Herz, M. B. Johnston, S. M. Morris, H. J. Snaith and M. K. Riede, *Adv. Mater.*, 2016, **28**, 923-929.
16. P. Brenner, M. Stulz, D. Kapp, T. Abzieher, U. W. Paetzold, A. Quintilla, I. A. Howard, H. Kalt and U. Lemmer, *Appl. Phys. Lett.*, 2016, **109**, 141106.
17. B. Gholipour, G. Adamo, D. Cortecchia, H. N. Krishnamoorthy, M. D. Birowosuto, N. I. Zheludev and C. Soci, *Adv. Mater.*, 2017, **29**, 1604268.
18. S. V. Makarov, V. Milichko, E. V. Ushakova, M. Omelyanovich, A. Cerdan Pasaran, R. Haroldson, B. Balachandran, H. Wang, W. Hu, Y. S. Kivshar and A. A. Zakhidov, *ACS Photonics*, 2017, **4**, 728-735.
19. H. Wang, R. Haroldson, B. Balachandran, A. Zakhidov, S. Sohal, J. Y. Chan, A. Zakhidov and W. Hu, *ACS Nano*, 2016, **10**, 10921-10928.
20. N. Cefarin, A. Cian, A. Sonato, E. Sovernigo, F. Suran, Z. Teklu, A. Zanut, A. Pozzato and M. Tormen, *Microelectron. Eng.*, 2017, **176**, 106-110.
21. N. Pourdavoud, S. Wang, A. Mayer, T. Hu, Y. Chen, A. Marianovich, W. Kowalsky, R. Heiderhoff, H. C. Scheer and T. Riedl, *Adv. Mater.*, 2017, **29**, 1605003.
22. B. Jeong, I. Hwang, S. H. Cho, E. H. Kim, S. Cha, J. Lee, H. S. Kang, S. M. Cho, H. Choi and C. Park, *ACS Nano*, 2016, **10**, 9026-9035.
23. J. Mao, W. E. I. Sha, H. Zhang, X. Ren, J. Zhuang, V. A. L. Roy, K. S. Wong and W. C. H. Choy, *Advanced Functional Materials*, 2017, **27**, 1606525.
24. M. A. Verschuuren, Ph. D. thesis, Utrecht University, 2010.
25. H. Schmid and B. Michel, *Macromolecules*, 2000, **33**, 3042-3049.
26. F. Hua, A. Gaur, Y. Sun, M. Word, N. Jin, I. Adesida, M. Shim, A. Shim and J. A. Rogers, *IEEE Trans. Nanotech.*, 2006, **5**, 301-308.
27. B. D. Gates and G. M. Whitesides, *Journal of the American Chemical Society*, 2003, **125**, 14986-14987.
28. Z. Hu, G. Baralia, V. Bayot, J.-F. Gohy and A. M. Jonas, *Nano Lett.*, 2005, **5**, 1738-1743.
29. S. Brittman and E. C. Garnett, *J. Phys. Chem. C*, 2016, **120**, 616-620.
30. A. H. Schokker and A. F. Koenderink, *Phys. Rev. B*, 2014, **90**, 155452.
31. S. A. Mann, B. Sciacca, Y. Zhang, J. Wang, E. Kontoleta, H. Liu and E. C. Garnett, *ACS Nano*, 2017, **11**, 1412-1418.

32. M. Xiao, F. Huang, W. Huang, Y. Dkhissi, Y. Zhu, J. Etheridge, A. Gray-Weale, U. Bach, Y. B. Cheng and L. Spiccia, *Angew. Chem. Int. Ed. Engl.*, 2014, **53**, 9898-9903.
33. M. A. Lieb, J. M. Zavislan and L. Novotny, *J. Opt. Soc. Am.*, 2004, **21**, 1210-1215.
34. H. Kogelnik and C. V. Shank, *J. Appl. Phys.*, 1972, **43**, 2327-2335.
35. L. A. Coldren, S. W. Corzine and M. L. Masanovic, *Diode Lasers and Photonic Integrated Circuits*, John Wiley & Sons, Hoboken, New Jersey, 2nd Edition edn., 2012.
36. M. B. Price, J. Butkus, T. C. Jellicoe, A. Sadhanala, A. Briane, J. E. Halpert, K. Broch, J. M. Hodgkiss, R. H. Friend and F. Deschler, *Nat. Commun.*, 2015, **6**, 8420.

Electronic Supplementary Information for

Controlling Crystallization to Imprint Nanophotonic Structures into Halide Perovskites Using Soft Lithography

Sarah Brittman, Sebastian Z. Oener, Ke Guo, Haralds Āboliņš, A. Femius Koenderink, and Erik C. Garnett*
Center for Nanophotonics, AMOLF, Science Park 104, Amsterdam 1098 XG, the Netherlands

*Corresponding author: garnett@amolf.nl

Estimated refractive indices and mode indices of the waveguide

The waveguide structure consists of a film 140 nm thick underneath a corrugation that is 50 nm deep. First an effective refractive index for the layer was approximated. The value of the refractive index (*n)* of the perovskite at 543 nm was taken to be 2.25.[1] To approximate the effective refractive index, the layer was considered a stack of two layers:

(1) 50 nm layer with an index determined by its 50% fill fraction:

$$1.74 = \sqrt{0.5 * 2.25^2 + 0.5 * 1^2}$$

(2) 140 nm layer with an index of 2.25.

The low-index layer is then 26% of the total thickness, so the combined index is estimated as $2.13 = \sqrt{0.74 * 2.25^2 + 0.26 * 1.74^2}$.

Then the mode indices of the TE and TM waveguide modes of a 190-nm layer with this refractive index (*n*=2.13) on a fused silica substrate (*n*=1.46) were calculated from equations 4.4 and 4.17 in

Urbach, H. P. and Rikken, G. L. J. A. Spontaneous Emission for a Dielectric Slab. *Phys. Rev. A*, 1998, 57, 3913-3930.

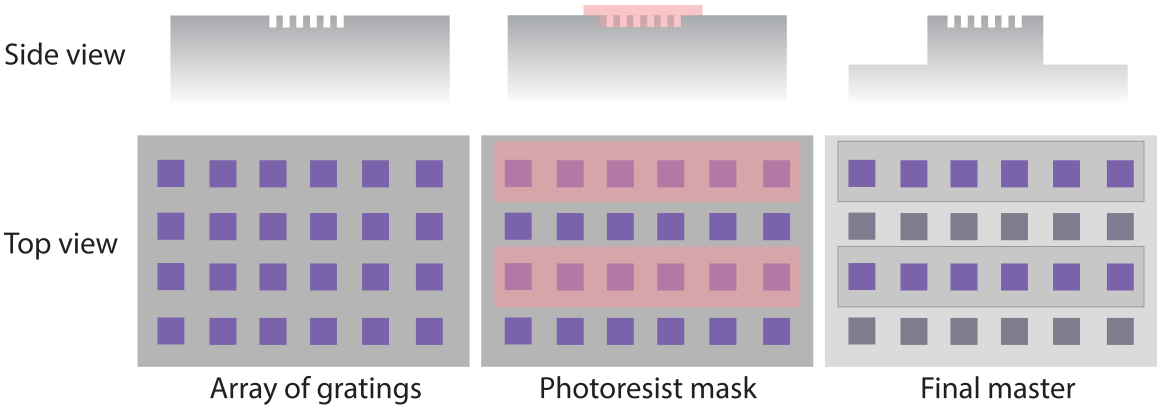

Fig. S1 Scheme of creating the waveguide underneath the gratings in the silicon master. After an array of gratings was etched in the silicon, specific lines of the array were protected by photoresist. All the unprotected silicon is etched away, leaving lines of gratings on top of an underlying waveguide. The unprotected gratings were damaged and not used. This scheme was applied for expediency - simply to reuse an existing photolithography mask on hand.

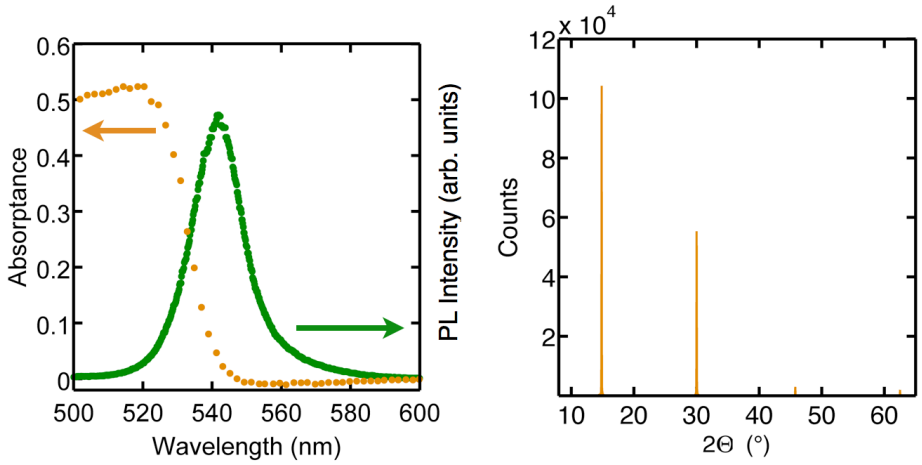

Fig. S2 Absorptance, photoluminescence, and X-ray diffraction of the $CH_3NH_3PbBr_3$ film.

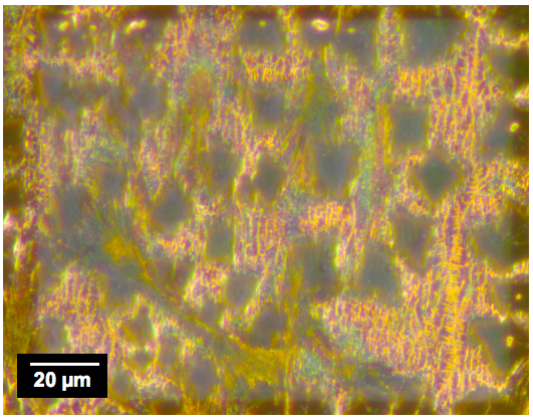

Fig. S3 Isolated crystals and wire-like structures that form because there is too much solvent in the film when it is imprinted.

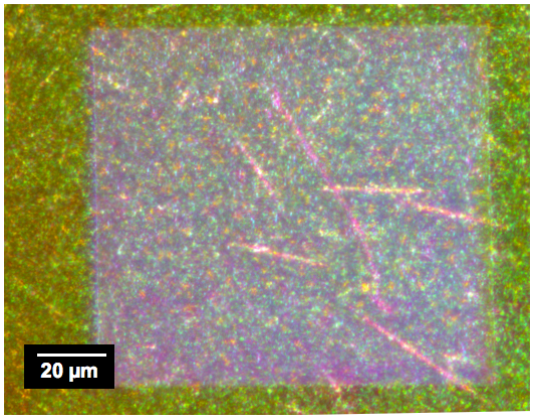

Fig. S4 Weak imprinting from too little solvent present for the array to fully recrystallize in contact with the stamp. Note the scattering of the array and lack of a highly uniform color from diffraction.

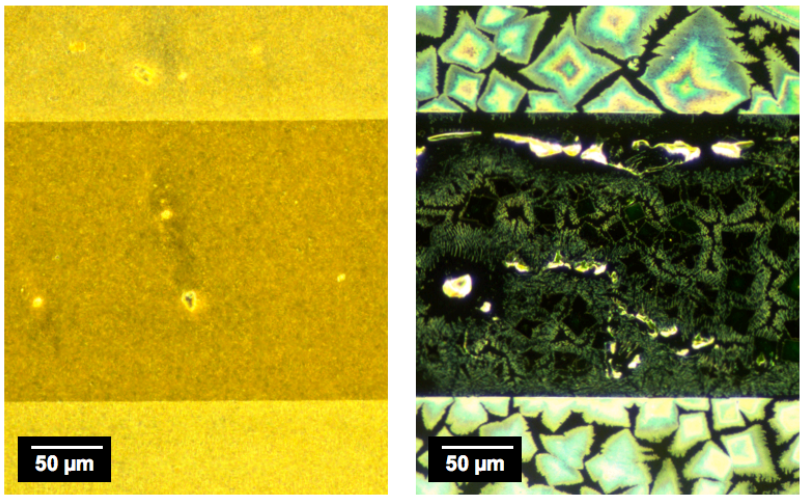

Fig. S5 Isolated crystals form underneath the stamp when there is too much solvent from precursors in pure DMF (right). A continuous film forms when the solvent is removed before imprinting (left). The top and bottom bands are the patterned regions, while the center band is unpatterned. The patterns here are inverse nanoscale pyramids, not gratings.

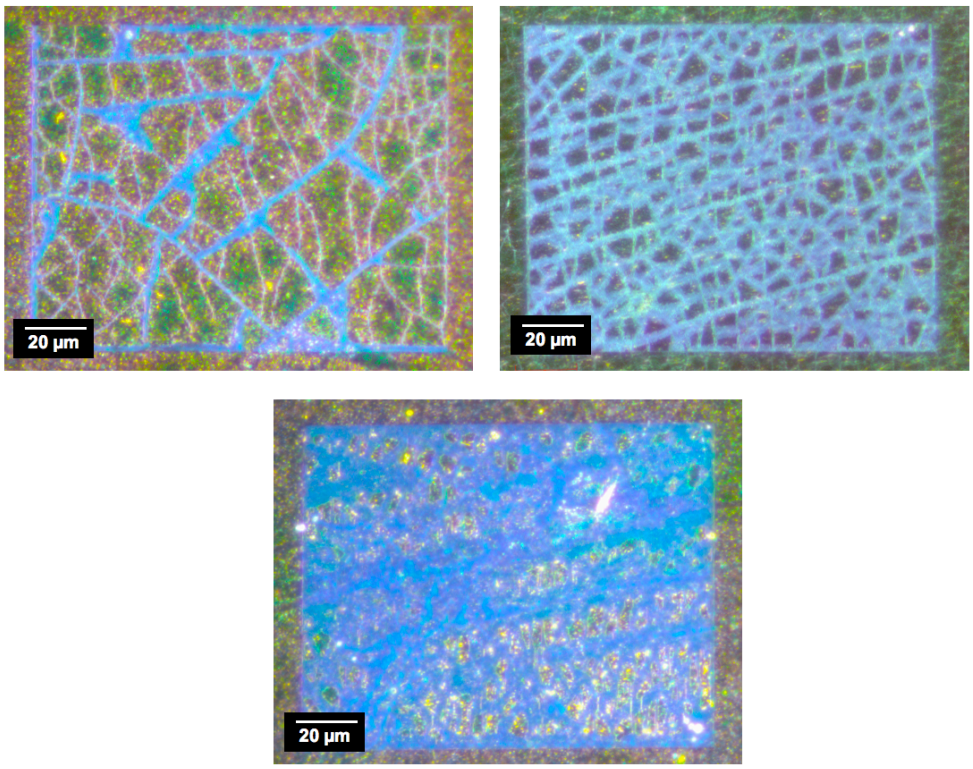

Fig. S6 Increasing crystallization of the grating with a decrease in the time of the pre-annealing step. Longer pre-annealing removes the solvent that facilitates recrystallization.

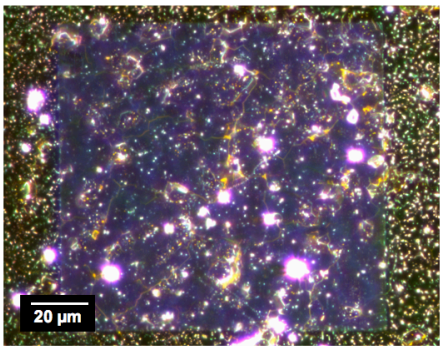

Fig. S7 $CH_3NH_3PbBr_3$ grating imprinted using only DMSO

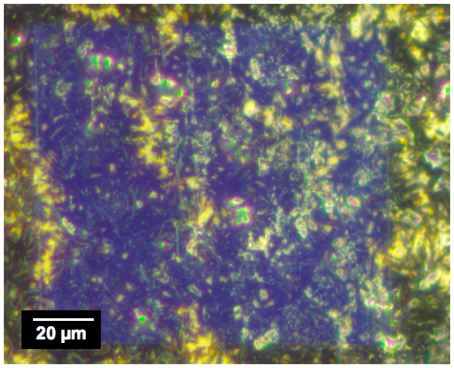

Fig. S8 $CH_3NH_3PbI_3$ grating from only DMSO. The 1 M precursor solution was made from a 1:1 ratio of PbI_2 (Aldrich) and CH_3NH_3I, which was synthesized and recrystallized from ethanol. For the iodide perovskite, no pre-annealing step was necessary. Rather, the precursor was spincoated to form a grayish intermediate that was then imprinted.

Lines			Gaps			Periodicity
Si master	Perovskite	Ratio	Si master	Perovskite	Ratio	Ratio
128	134	1.05	110	113	1.03	1.05
126	140	1.11	121	108	0.89	1.04
130	134	1.03	116	124	1.06	1.04
129	140	1.08	126	132	1.04	1.10
137	142	1.04	129	134	1.04	1.08
148	169	1.15	129	121	0.94	1.09
159	164	1.03	129	137	1.06	1.09
164	191	1.16	134	126	0.94	1.10
175	199	1.14	132	124	0.94	1.08
164	194	1.18	153	140	0.91	1.09

Table S1 Comparison of dimensions (in nm) of the lines and air gaps in the silicon master and the perovskite gratings, which were imprinted from the mixed DMF-DMSO precursor. The total periodicity of the structures is about 4-10% larger in the perovskite than in the silicon masters, likely from the tension in the PDMS stamp.